Epitaxial II–VI Tripod Nanocrystals: A Generalization of van der Waals Epitaxy for Nonplanar Polytypic Nanoarchitectures

Muhammad Iqbal Bakti Utama,[†] Qing Zhang,[†] Shuangfeng Jia,[‡] Dehui Li,[†] Jianbo Wang,[‡,*] and Qihua Xiong[†,§,*]

[†]Division of Physics and Applied Physics, School of Physical and Mathematical Sciences, Nanyang Technological University, Singapore 637371, [‡]School of Physics and Technology, Center for Electron Microscopy and MOE Key Laboratory of Artificial Micro- and Nano-structures, Wuhan University, China 430072, and [§]Division of Microelectronics, School of Electrical and Electronic Engineering, Nanyang Technological University, Singapore 639798

ABSTRACT

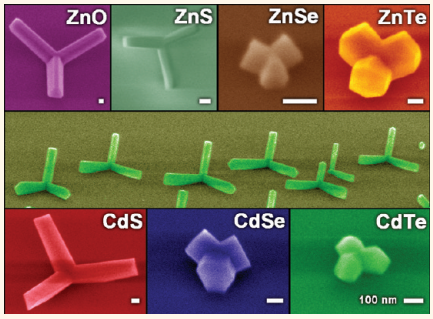

We report for the first time the synthesis of nonplanar epitaxial tripod nanocrystals of II–VI compounds (ZnO, ZnS, ZnSe, ZnTe, CdS, CdSe, and CdTe) on muscovite mica substrate. With CdS as a case study, we conclude *via* Raman spectroscopy and electron microscopy studies that the tripods, which are found to be polytypic, followed a seeded growth mechanism. The epitaxy, manifested by the in-plane alignment of the legs of the tripods within a substrate, is attributed to the van der Waals interaction between the tripod bases and the mica surface, instead of to the covalent chemical bond which would require lattice matching between the epilayer and the substrate. The results demonstrated herein could have widespread immediate implications, including the potential of van der Waals epitaxy to be applicable in producing ordered arrays of more complex nanoarchitectures from various classes of compounds toward a broad range of technological applications.

KEYWORDS: van der Waals epitaxy · heteroepitaxy · II–VI semiconductor · muscovite mica · nanostructures · nanotripods

The advent of the bottom-up paradigm as a prospective alternative of miniaturization for technological advancement led to the intensive exploration of routes to prepare semiconductor nanostructure as the building blocks of functional devices.[1,2] Central to the paradigm is the ability to produce and manipulate nanostructures into a specific morphology and size to achieve the desired properties and functionalities, which has been accomplished by synthesizing crystals in various shapes.[3–6] Of comparable importance, albeit less commonly addressed, is the feasibility to organize the structures into ordered assemblies, which is crucial for the integration into reliable devices.[7,8] *In situ* growth of a crystal array on a substrate *via* epitaxial growth is the most direct approach to accomplish such organization at high-throughput. However, the option of materials and structures that can be prepared in epitaxial growth has been limited by the availability of a suitable substrate, which requires lattice matching and similarity in crystal symmetry to avoid undue accumulation of strain and defects.[9]

van der Waals epitaxy has been proposed to circumvent the lattice matching requirement for epitaxial growth by utilizing layered substrates, whose basal cleavage surface is free of dangling bonds and is thus inert.[10] Hence, the heterojunctions will primarily be connected by van der Waals interaction instead of chemical bonding, enabling the growth of monocrystalline film from various compounds irrespective of their lattice mismatch to the substrate. Yet despite its potential, van der Waals epitaxy for inorganic nanostructures has only been attributed in the growth of single-phased conformal and planar structures,[11,12] with demonstration[13,14] and elucidation[15] in vertically aligned semiconductor nanowire arrays reported only very recently.

We report an extension of the van der Waals epitaxy by synthesizing—for the first time—epitaxial tripods of II–VI semiconductors

* Address correspondence to wang@whu.edu.cn, qihua@ntu.edu.sg.

Received for review November 9, 2011 and accepted February 20, 2012.

Published online February 21, 2012
10.1021/nn204344z

(ZnO, ZnS, ZnSe, ZnTe, CdS, CdSe, and CdTe). Muscovite mica is used as the substrate, as it has been previously demonsrated to be capable of manifesting the van der Waals epitaxy in other structures.[13,16−19] Notably, our one-step vapor transport approach yields nearly selective production of branched crystals in the tripodal form (*i.e.*, three-fold symmetrically branched legs protruding from a common center), whereas past syntheses of a branched-leg crystal had mainly resulted in freestanding and colloidal tetrapods[20−26] or a mixture of multipods (*e.g.*, nanorods, dipods, and tripods).[27−33] Such utilization of van der Waals epitaxy to synthesize epitaxial nanoarchitectures with high complexity—in comparison to the simpler thin film and nanowire structures—may thus serve as a milestone for future explorations toward simultaneously attaining control of morphology and preparing an ordered array of nanostructures using a generic growth strategy that is applicable to various compounds.

RESULTS AND DISCUSSION

Scanning electron microscopy (SEM) revealed that the tripods exhibited morphological features unique to the constituent compound (Figure 1 and Figures S2 and S3 in Supporting Information), as exemplified by the flat-faceted legs of the triangular cross section from CdS reminiscent to that of vertical CdS nanowires on mica (Figure S5). The tripod legs were typically upward-inclined, interfacing the substrate only close to the tripod center without a buffer layer or any intermediate structures.

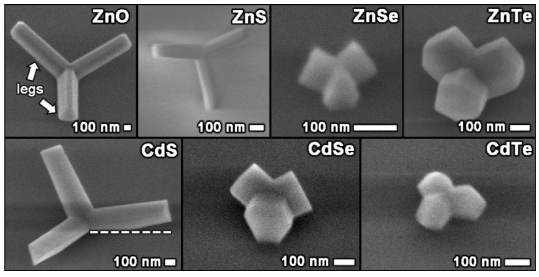

Figure 1. SEM images in 45° inclined view of individual II−VI tripods on muscovite mica substrate. The white arrows near the ZnO tripod point to the protrusions which are referred to as the "legs" of the tripod. Meanwhile, the dashed line on the CdS tripod is a guide to show that the tripod legs are inclined from the substrate.

The majority of tripods are preferentially oriented in only two directions which are related by a 60° rotation, assuming that the three legs are morphologically identical (Figure 2a,b and Figures S1−S3). Such in-plane alignment of the tripods strongly indicates that the tripods are grown epitaxially from the substrate. In-plane alignment is a consequence of both (i) the consistency in the relationship of atomic ordering between the substrate and all of the nanostructures (*i.e.*, the presence of epitaxy); and (ii) the correlation between crystallinity and morphological construct of the nanostructures (further discussion regarding this point is provided to accompany Figure 4 and 5). Besides, in-plane alignment between neighboring epitaxial nanostructures had also been exhibited by the faceting of the nanowire array[15,34] and the branching of nanotrees.[6]

There are two possible ways for achieving the epitaxy between two contacting solids: (i) *via* the chemical bonding between the atoms of the two solids, which is a very well-established mechanism and can be typically found in a conventional bulk system;[35] or (ii) *via* the van der Waals attraction between the dipoles (which could be permanent or induced) across the surface of the two solids.[10] In other words, van der Waals epitaxy is an epitaxy where there is only very little to no bonding between the epitaxial structure to the substrate, as opposed to the con-

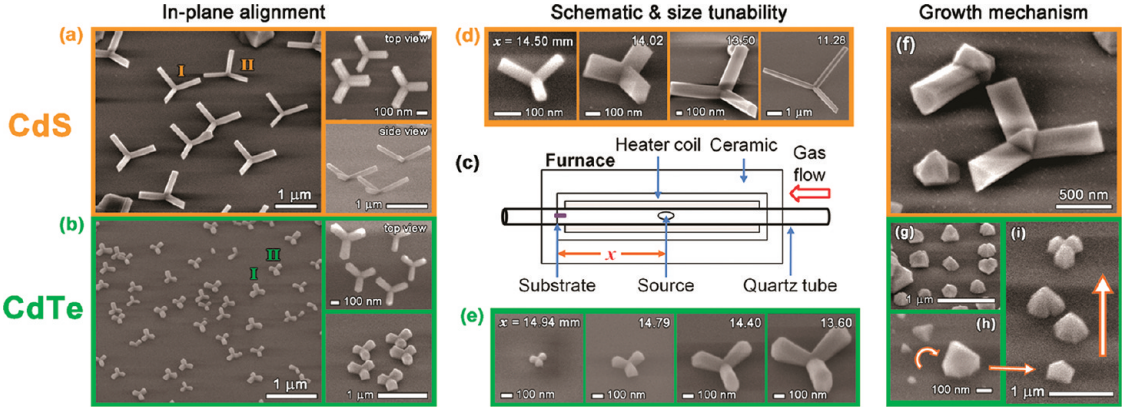

Figure 2. SEM characterizations of the as-synthesized tripods from CdS (upper half, with orange bordering) and CdTe (lower half, green bordering) as the representative of II−VI compounds. Unless otherwise indicated, the images were recorded in a 45° inclined view. (a,b) In-plane alignment of tripods. Instances of the two possible orientations are marked with "I" and "II", respectively. (c) Schematic of the synthesis setup. (d,e) Position-dependent size of the tripods. The number on the top right corner of the images is the spacing between the position of the tripod on the substrate with the center of the furnace during the synthesis, in millimeters, as denoted by "*x*" in (c). (f−i) Incomplete tripods and pyramidal particles, revealing information about the growth mechanism of the tripods. The arrows indicate the direction of successive growth stages that are represented by the structures.

ventional epitaxy which is due to chemical bonds. As a major advantage of van der Waals epitaxy, lattice matching is not essential for the epitaxial growth.[11] This situation is in contrast to that in conventional epitaxy, where the much stronger chemical bonds (when compared to van der Waals force) between the epitaxial material and the substrate will strain the epitaxial material to cause defects which disrupt the atomic ordering when the lattice mismatch is too high.[9,35] It is indeed true that, conceptually, lattice-mismatched epitaxial growth of nanostructures—particularly in nanowires[36,37]—could indeed be aided by radial/lateral strain relaxation owing to their limited radial dimension. However, such strain relaxation capability is still very limited and nevertheless strongly dependent on lattice mismatch. The lack of previous reports on the epitaxial growth of nanotripods, as other synthesis works on tripods had generally resulted in freestanding product (*i.e.*, detached from any substrate), thus suggests that such lattice matching constraint in conventional heteroepitaxy is also effective in tripod nanostructures despite the presence of lateral relaxation.

We then argue that the growth of II–VI tripods reported herein can be attributed to the van der Waals epitaxy. First, we had intentionally invoked the epitaxy mechanism by using the freshly cleaved muscovite mica substrate, which had also previously been used in the demonstration of van der Waals epitaxy of other structures.[13,16–19] The choice of muscovite mica is motivated by its layered structure, as layered materials (*e.g.*, mica, transition metal dichalcogenides) have their layers connected by a van der Waals attraction instead of chemical bonds. Thus, an as-exfoliated fresh surface of layered materials will be free of dangling bonds and is not expected to form chemical bonds required in the conventional heteroepitaxy.[10]

Second, the absence of a buffer layer or any intermediate structures suggests that the growth is not of the conventional heteroepitaxy category. The buffer layer is commonly defect-rich and is formed to relieve the strain in nanostructures from highly lattice-mismatched conventional heteroepitaxy. As had been elucidated in the case of nanowires,[38] the extent of such a buffer layer manifestation onto the base of the nanostructures thus depends on the amount of strain energy to be released, which is a function of the lattice mismatch and size of the structure, among others. As such, the appearance of a buffer layer in nanowires (and other nanostructures) may also range from an elaborate network of thin structure for a highly mismatched system to an evident bulging or an intermediate structure only at the base of a wire.[38] Thus, the absence of a buffer layer in all of our epitaxial II–VI tripods implies that there is not much strain energy to be relaxed in the system. This observation cannot be explained in terms of conventional heteroepitaxy as we should expect a presence of lattice mismatch between the various II–VI compounds to the muscovite mica substrate, due to the inevitable variation of lattice parameters—especially those which are in-plane—of each II–VI compound relative to that of mica. Therefore, this result implies that lattice matching between the epilayer and the substrate is not required for the epitaxy, in accordance to the advantage of the van der Waals epitaxy over the conventional heteroepitaxy.

The tripods within a local area (~0.1 mm^2) of the substrate are of approximately uniform size (Figure S1). However, the size (length and circumference) of the CdS and CdTe legs correlates negatively with the spacing between the observation site on the substrate and the center of the furnace setup, regardless of whether the observation sites are on the same substrate (CdTe, note the alignment in Figure 2e) or on substrates from different growth batches (CdS, Figure 2d). The position-dependent size presents the opportunity for rational size tuning, which might be exploitable to meet technological demand.

Another feature of our synthesis method is the occasional presence of small pyramid-like crystals and incomplete tripods (possessing only one or two legs) near the side edges and at the more downstream position of the substrate (Figure 2f–h), where the local reactant vapor supply and temperature can be expected to be suboptimal. Interestingly, unobstructed fragment of the pyramidal crystals can be recognized at the branch point of the incomplete tripods, which had already conformed to the in-plane alignment (Figure 2f and Figure S4). We conclude that the pyramidal crystals are actually the seed for tripod growth (Figure 2i) and are responsible for the epitaxy with the substrate.

Three mechanisms have been proposed on seeded growth of branched-leg semiconductor crystals, with the ZnO tetrapod as the prototype, by considering the phase of the seed. The first mechanism is based on a polytypic model, where legs in the hexagonal wurtzite (WZ) phase are growing along ⟨0001⟩ on a specific set of {111} facets of the octahedral seed in the cubic zinc-blende (ZB) phase.[39] The second mechanism accounts for complete WZ structure, where the seed is of octahedral multi-inversion twins composed by eight trigonal pyramids with a $\{0001\}_{WZ}$ and three $\{11\bar{2}2\}_{WZ}$ planes.[40] Meanwhile, the third mechanism assumes a phase transformation of the less stable ZB nucleus into a WZ multi-twinned seed.[41] Although the majority of solution-based syntheses adopted the first mechanism, reports on vapor-based syntheses with the first two mechanisms are more balanced. Both mechanisms have been corroborated by morphological consideration, selected area electron diffractometry (SAED), and high-resolution transmission electron microscopy (HRTEM).[42,43]

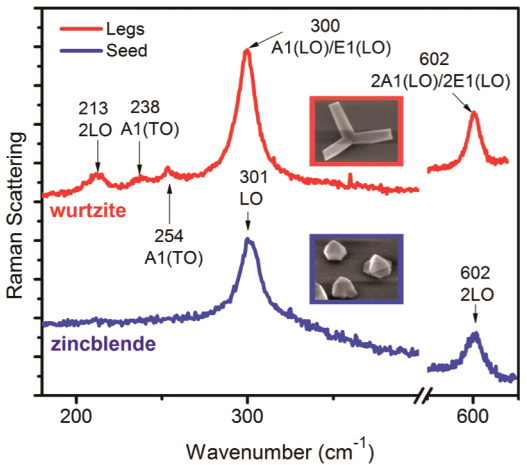

Figure 3. Raman spectra from a tripod leg (red) and a seed particle (blue), which can be identified as WZ and ZB phases, respectively.

ZB was found to be the stable phase for freestanding bulk II−VI compounds, except for CdS and ZnO which are more stable in WZ.[44] However, epitaxial growth may distort the stability and preferred nucleation phase. We therefore focus our attention to CdS to determine whether the ZB phase could persist on mica for the feasibility of the polytypic growth mechanism.

Micro-Raman spectroscopy has been widely utilized to characterize various crystallinity-related phenomena of nanostructures.[45−48] We propose a method for rapid evaluation of the growth mechanism by comparing the micro-Raman spectra from a leg of a tripod and a seed crystal (for CdS, Figure 3, or the junction of the legs for ZnO, Figure S8) to distinguish the spectroscopic characters between ZB and WZ phases. While the LO modes of ZB and WZ CdS are known to coincide, A1(TO) phonon in CdS is a mode exclusive to the WZ phase.[49] Thus, the absence of A1(TO) phonon in the spectrum of the CdS seed suggests that pristine ZB phase of CdS may indeed nucleate on the mica surface.

We then collected SAED patterns from the top view of a CdS tripod, whose bright-field TEM images (Figure 4a,b) showed a nearly 120° angle between the projection of adjacent upward-inclined legs on the viewing plane. In addition to the superimposition of the diffraction spots from the three legs, where each can be indexed to the $[3\bar{3}01]_{WZ}$ zone axis (Figure 4d−f), an extra set of spots was detected from the center of the tripod (Figure 4c). The extra spots can be uniquely indexed to $[\bar{1}\bar{1}\bar{1}]_{ZB}$ zone axis, confirming the existence of the ZB phase. As the zone axis, which is directed outward from the plane of the paper, is antiparallel to the base of the tripod, we concluded that the $\{111\}_{ZB}$ facet was the plane forming the heteroepitaxy with the substrate.

We also examined a tripod with a missing leg (Figure 4g) to allow HRTEM imaging at a thinner region of the tripod center. The orientation was made such that the remaining legs laid flat within the same

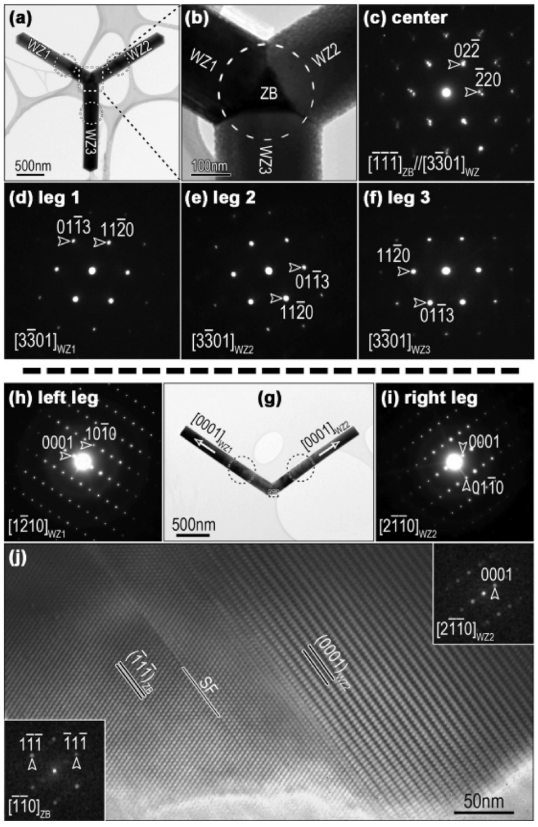

Figure 4. Bright-field TEM and SAED characterizations of a complete tripod (a−f) and a broken tripod (g−j) of CdS in top view and side view, respectively. Indexing of the SAED of the tripods at the center (c) confirmed the presence of a ZB seed at the junction of the three WZ legs (d−f), as summarized with the labeling in (a) and (b). The SAED patterns of the legs in side view (h,i) show that the legs grew along $[0001]_{WZ}$ with $\{2\bar{1}\bar{1}0\}_{WZ}$ side facets. (j) HRTEM at the junction of a broken tripod, displaying the epitaxy between the seed and the right leg which is accompanied by a stacking fault (SF). Inset: FFT of the seed (bottom left) and the right leg (top right), revealing an epitaxial relationship of $(\bar{1}1\bar{1})\langle\bar{1}10\rangle_{ZB}||(0001)\langle2\bar{1}\bar{1}0\rangle_{WZ}$ between the seed and the leg.

viewing plane. The beam axis coincided with one side facet of the legs, which is of $\{2\bar{1}\bar{1}0\}_{WZ}$, and the growth direction of the legs is determined to be along $[0001]_{WZ}$. The presence of the ZB seed was verified unambiguously (Figure 4j). The epitaxial relationship of $(\bar{1}1\bar{1})\langle\bar{1}10\rangle_{ZB}||(0001)\langle2\bar{1}\bar{1}0\rangle_{WZ}$ between the seed and the legs can be deduced from the fast Fourier transform (FFT) patterns of the seed and the right leg (insets in Figure 4j). Stacking fault (SF) was also produced due to the change in stacking sequence from ABCABC in ZB to ABAB in WZ during the phase transformation to stabilize the structure. As the ZB seed is smaller than the diameter of the WZ leg, which is evidenced by the concealment of the seed on a typical tripod, the WZ legs were contacted at an angle of ~110.8° to form a twin structure with $(01\bar{1}3)$ interface plane (Figure S9).

For compounds of $M^{II}E^{VI}$ type, the $\{111\}_{ZB}$ and $\{0001\}_{WZ}$ surfaces are polar due to the difference in

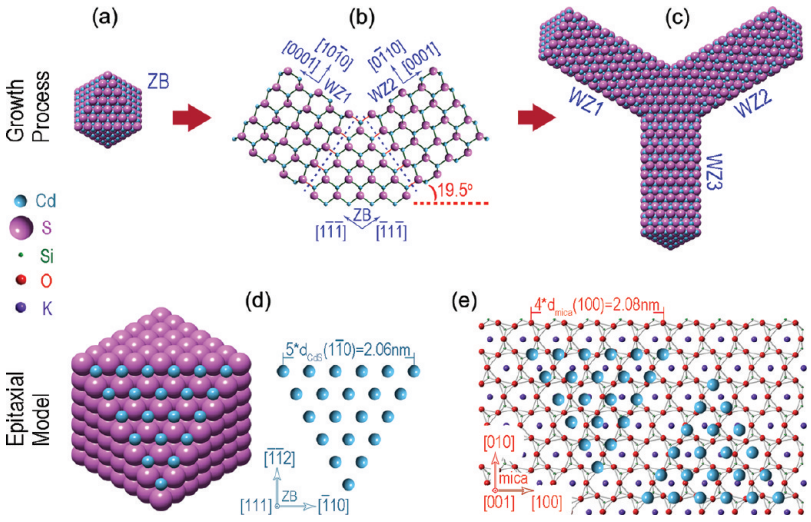

Figure 5. Atomic modeling of growth process (upper half) and epitaxy (lower half) for CdS tripods. (a) Top view of a ZB octahedral seed crystal. (b) Side view of epitaxial growth of inclined WZ legs on the seed. (c) Top view of a complete tripod. (d) Bottom view of the seed, showing triangular $(111)_{ZB}$ base. (e) Two possible arrangements of Cd atoms from the triangular base of the seed crystal, in order to match the crystalline symmetry of the mica surface.

electronegativity of M atoms (which then become M^{2+} cations) and E atoms (E^{2-}, anions). The growth kinetics and morphology of II−VI crystals, which are otherwise formed in the same phase, are strongly dependent on the polarity of the facets.[50] Given the similar morphology of the legs of the tripods and of the vertically aligned nanowires of CdS and ZnO, the latter of which were grown on mica in WZ along $+[0001]_{WZ}$ (Figure S5), we presume that the legs of tripod and nanowire share identical crystal polarity. Therefore, the legs of CdS and ZnO tripods should also grow along $+[0001]_{WZ}$, which results in a cation-terminated end facet. As the base of the legs are epitaxially related to the $\{111\}_{ZB}$ facets of the seed (Figure 3i), we also deduce that the legs are grown only on the cation-terminated $+\{111\}_{ZB}$ surfaces of the seed. Furthermore, taking into account the {111} octahedron habit of the seed crystal for the polytypic growth mechanism[39] and the upward-inclined legs from the substrate, the base of the seed should also be a cation-terminated $+\{111\}$ surface.

Herein, we recapitulate the growth process with CdS as a case study. At the optimal growth environment of tripods (Figure S1), after considering the influence of substrate, the energy difference between WZ and ZB is sufficient to favor nucleation in the ZB phase,[44] where the base of the seed is the Cd-terminated $(111)_{ZB}$ (Figure 5a,d). During the subsequent growth of the heteronucleated ZB seed, the phase stability may be reversed to minimize surface energy contribution to the total energy, which are increasingly significant in the nanoscale.[43] Phase transformation of ZB to WZ for the growth of legs may then proceed once the $\pm\{111\}_{ZB}$ surfaces are exposed, when the seed crystal had ideally attained a regular octahedron habit (Figure 5a), due to their equivalence to $\pm(0001)_{ZB}$ surfaces. However, the three WZ legs grow only on the three remaining $+\{111\}_{ZB}$ surfaces (*i.e.*, $1\bar{1}\bar{1}$, $\bar{1}1\bar{1}$, $\bar{1}\bar{1}1$) along the cation-terminated $+[0001]_{WZ}$ (Figure 5b) to result in tripod with ~19.5° upward-inclined legs (Figure 5c), instead of tetrapod which is more commonly reported in the literature.[20−26] Do note that the growth mechanism of the tripods is distinct from the multiple-order twinning seed model to explain the presence of nonvertical nanowires[51] where, despite the growth is also proposed to start from an octahedral ZB seed, it is common to observe only single wires—which preserve their ZB phase—to protrude from the first-order seed, thus also resulting in ~19.5° inclination.

It is very likely that the nucleation and growth rate of legs along $+[0001]_{WZ}$ is significantly higher than that of the anion-terminated $-[0001]_{WZ}$ legs on the $-\{111\}_{ZB}$ surfaces (*i.e.*, $\bar{1}\bar{1}\bar{1}$, $\bar{1}11$, $1\bar{1}1$, $11\bar{1}$). For WZ ZnO, the $[0001]_{WZ}$ is indeed the favorite growth direction, which was attributed to the high effective surface energy of Zn^{2+} planes due to the severe straining on their surface atomic bonds.[52] The cation-terminated surfaces of vapor-phase grown CdSe, ZnS, and ZnO is also known to be catalytically active, while the anion-terminated surface is inactive.[53] Additionally, the $+[0001]_{WZ}$ growth-directed CdS tripod legs with $\{2\bar{1}\bar{1}0\}_{WZ}$ side facets (Figure 4i) is consistent with the reported habit of pure CdS needles[54,55] grown with vapor-based technique at 700−800 °C, which encloses the temperature range used in our synthesis.

The approximately equal length of legs from the majority of tripods indicates that the faceting of the seed is uniform, with the exposure of all $\pm\{111\}_{ZB}$ facets of the octahedral seed and the subsequent phase transformation occurring near concurrently. Exception occurs on the aforementioned regions with suboptimal environment. The seed pyramidal crystals,

isolated or remaining at the junction of incomplete tripods, were often found with extra facets or underdeveloped $+\{111\}_{ZB}$ facets (Figure S6), which may explain the failure to grow the legs properly.

The preferential orientation of tripod legs could be elucidated in the context of van der Waals epitaxy. Muscovite mica surface is constructed by sheets of SiO_4 tetrahedra and octahedra linked by a layer of K^+ ions which are positioned on top of the pseudohexagonal arrangement of the oxygen atoms. A quarter of the silicon sites is occupied by Al^{3+} instead of Si^{4+} ions, creating interlayer dipoles between K^+ and AlO_4^- which remain as surface dipoles upon cleavage.[56] Attractive van der Waals interaction may therefore occur between the mica surface dipole and the downward-pointing permanent dipole on the base of the $+(111)_{ZB}$ seed particle, where the strongest attraction occurs when the Cd^{2+} (or Zn^{2+}) ions are close to the oxygen ions of mica. Although a large lattice mismatch is present between the (001) plane of muscovite and $+(111)_{ZB}$ plane of II–VI, their crystalline symmetry is similar and can be exploited to increase the frequency of proximity between the II–VI cations and oxygen atoms. For CdS (Figure 5d,e), the epitaxial growth of the seed in such a scenario would commence by $(001)\langle 100\rangle_{mica}\|(\bar{1}\bar{1}1)\langle 1\bar{1}0\rangle_{ZB}$, similar to that of CdS film on mica.[57] Since the lattice of the seed is relaxed due to the van der Waals epitaxy, the ~20.8% lattice-mismatched $(100)_{mica}$ and $(1\bar{1}0)_{ZB}$ planes are incommensurate as indicated by the absence of any heavily strained intermediate structures or buffer layer. However, proximity of the planes may occur every $4d_{mica}(100)$ and $5d_{CdS}(1\bar{1}0)$ to allow for the epitaxy anchoring. Considering that the octahedral seed crystal has equilateral triangular facets, the seed may grow epitaxially with its base oriented in two possible antiparallel directions (Figure 5e) which are manifested as the two preferential orientations of the CdS tripod legs.

CONCLUSIONS

We have reported the synthesis of epitaxial polytypic II–VI tripods for the first time and discussed the growth mechanism of the structure. Our study demonstrated the general applicability of the mica substrate, which could invoke van der Waals epitaxy, to grow epitaxial complex nanoarchitectures from a wide range of materials to provide richer opportunities of fundamental studies and technological applications. While their intrinsic material properties might be similar, we expect that epitaxial tripods and tetrapods exhibit superior prospect to that of freestanding and colloidal branched-leg structures. For example—also an instance of possible future direction of research derived from our works—the attachment of epitaxial tripods to the substrate with van der Waals epitaxy might be exploited in the production of an ordered array *via* positioning control to achieve a rational fabrication of reliable devices. We believe that particular emphasis might be given to the development of optoelectronic devices based on these tripods, especially since II–VI nanostructures had been demonstrated to have fascinating crystalline and optical properties.[58]

METHODS

Synthesis. The II–VI tripods were synthesized using a vapor transport system, where the schematic of the setup is shown in Figure 2b. A sheet of (001) muscovite mica $[KAl_2(Si_3Al)O_{10}(OH)_2$, muscovite-$2M_1$, research grade][15] was cut into pieces with typical size of 2 cm × 0.5 cm and air-cleaved without any surface treatment, to be used as the substrate with the freshly cleaved surface facing upward. The substrate was positioned downstream inside a quartz tube mounted on a single zone furnace (Lindberg/Blue M TF55035C-1), with its upstream edge at a distance of 12–16 cm from the center of the furnace. The powder of the material to be synthesized (ZnO, 99.99%, Alfa Aesar; ZnS, 99.99%, Alfa Aesar; ZnSe, 99.99%, Strem Chemicals; ZnTe, 99.99%, Alfa Aesar; CdS, 99.9%, Strem Chemicals; CdSe, 99.999%, Strem Chemicals; or CdTe, 99.99%, Aldrich Chemistry) was placed into a quartz boat which is located in the center of the furnace. For the synthesis of tripod structures shown in Figure 1, the vapor transport system was evacuated to the base pressure of ~2 mTorr, after which 30 sccm of Ar gas premixed with 5% H_2 was flown to allow the system to stabilize at 50 Torr. The temperature of the furnace was thus elevated to a designated value of the corresponding material to be synthesized (ZnO, 750 °C; ZnS, 725 °C; ZnSe, 800 °C; ZnTe, 800 °C; CdS, 750 °C; CdSe, 775 °C; CdTe, 650 °C), kept constant for 30 min, and allowed to reach the room temperature naturally. We noted that the tolerable temperature range for tripod growth could be relatively wide, as observed to be larger than ±50 °C for CdS.

Microscopy Characterizations. The morphology of the as-synthesized samples was characterized with a field emission scanning electron microscope (FE-SEM, JEOL JSM-7001F). The CdS tripods on mica were subsequently ultrasonicated in isopropyl alcohol and dispersed onto a carbon lacey grid for transmission electron microscopy (TEM). The TEM observations in bright-field imaging and selected area electron diffractometry were performed using JEOL JEM-2010 (HT) TEM with LaB_6 filament. High-resolution TEM (HRTEM) characterizations were conducted with JEOL JEM-2010FEF (UHR) TEM equipped with field emission gun and in-column Omega energy filter system.

Raman Spectroscopy. Room-temperature Raman scattering spectroscopy was performed on the as-synthesized samples using a micro-Raman spectrometer (Horiba-JY T64000) in a backscattering configuration. The sample was excited with a laser wavelength appropriate for the material under observation. The backscattered signal was collected through a 100× objective and then dispersed by a 1800 g/mm grating under a triple subtractive mode. The spectra resolution was ~1 cm^{-1}, and the lowest possible wavenumber was 5 cm^{-1}.

Conflict of Interest: The authors declare no competing financial interest.

Acknowledgment. Q.X. acknowledges the strong support from the Singapore National Research Foundation (NRF-RF2009-06). A generous start-up grant support (M58110061) and the New Initiative Fund (M58110100) from Nanyang Technological University.

Supporting Information Available: Additional SEM images (Figures S1–S6); Raman spectroscopy (Figures S7 and S8); an additional HRTEM image (Figure S9). This material is available free of charge *via* the Internet at http://pubs.acs.org.

REFERENCES AND NOTES

1. Lieber, C. M.; Wang, Z. L. Functional Nanowires. *MRS Bull.* **2007**, *32*, 99–108.
2. Xia, Y. N.; Yang, P. D.; Sun, Y. G.; Wu, Y. Y.; Mayers, B.; Gates, B.; Yin, Y. D.; Kim, F.; Yan, Y. Q. One-Dimensional Nanostructures: Synthesis, Characterization, and Applications. *Adv. Mater.* **2003**, *15*, 353–389.
3. Choi, C. L.; Alivisatos, A. P. From Artificial Atoms to Nanocrystal Molecules: Preparation and Properties of More Complex Nanostructures. *Annu. Rev. Phys. Chem.* **2010**, *61*, 369–389.
4. Kumar, S.; Nann, T. Shape Control of II–VI Semiconductor Nanomateriats. *Small* **2006**, *2*, 316–329.
5. Wang, D. L.; Lieber, C. M. Inorganic Materials—Nanocrystals Branch Out. *Nat. Mater.* **2003**, *2*, 355–356.
6. Dick, K. A.; Deppert, K.; Larsson, M. W.; Martensson, T.; Seifert, W.; Wallenberg, L. R.; Samuelson, L. Synthesis of Branched 'Nanotrees' by Controlled Seeding of Multiple Branching Events. *Nat. Mater.* **2004**, *3*, 380–384.
7. Yu, G.; Cao, A.; Lieber, C. M. Large-Area Blown Bubble Films of Aligned Nanowires and Carbon Nanotubes. *Nat. Nanotechnol.* **2007**, *2*, 372–377.
8. Javey, A.; Nam, S.; Friedman, R. S.; Yan, H.; Lieber, C. M. Layer-by-Layer Assembly of Nanowires for Three-Dimensional, Multifunctional Electronics. *Nano Lett.* **2007**, *7*, 773–777.
9. Matthews, J. W.; Blakeslee, A. E. Defects in Epitaxial Multilayers: I. Misfit Dislocations. *J. Cryst. Growth* **1974**, *27*, 118–125.
10. Koma, A.; Sunouchi, K.; Miyajima, T. Fabrication and Characterization of Heterostructures with Subnanometer Thickness. *Microelectron. Eng.* **1984**, *2*, 129–136.
11. Koma, A. van der Waals Epitaxy for Highly Lattice-Mismatched Systems. *J. Cryst. Growth* **1999**, *201*, 236–241.
12. Jaegermann, W.; Klein, A.; Pettenkofer, C. Electronic Properties of van der Waals-Epitaxy Films and Interfaces. In *Electron Spectroscopies Applied to Low-Dimensional Materials*; Hughes, H. P., Starnberg, H. I., Eds.; Kluwer: Dordrecht, The Netherlands, 2002; Vol. 24, pp 317–402.
13. Utama, M. I. B.; Peng, Z.; Chen, R.; Peng, B.; Xu, X.; Dong, Y.; Wong, L. M.; Wang, S.; Sun, H.; Xiong, Q. Vertically Aligned Cadmium Chalcogenide Nanowire Arrays on Muscovite Mica: A Demonstration of Epitaxial Growth Strategy. *Nano Lett.* **2010**, *11*, 3051–3057.
14. Chen, R.; Utama, M. I. B.; Peng, Z. P.; Peng, B.; Xiong, Q. H.; Sun, H. D. Excitonic Properties and Near-Infrared Coherent Random Lasing in Vertically Aligned CdSe Nanowires. *Adv. Mater.* **2011**, *23*, 1404–1408.
15. Utama, M. I. B.; Belarre, F. J.; Magen, C.; Peng, B.; Arbiol, J.; Xiong, Q. Incommensurate van der Waals Epitaxy of Nanowire Arrays: A Case Study with ZnO on Muscovite Mica Substrates. *Nano Lett.* **2012**, submitted.
16. Saiki, K.; Ueno, K.; Shimada, T.; Koma, A. Application of van der Waals Epitaxy to Highly Heterogeneous Systems. *J. Cryst. Growth* **1989**, *95*, 603–606.
17. Ueno, K.; Saiki, K.; Shimada, T.; Koma, A. Epitaxial Growth of Transition Metal Dichalcogenides on Cleaved Faces of Mica. *J. Vac. Sci. Technol., A* **1990**, *8*, 68–72.
18. Steinberg, S.; Ducker, W.; Vigil, G.; Hyukjin, C.; Frank, C.; Tseng, M. Z.; Clarke, D. R.; Israelachvili, J. N. van der Waals Epitaxial Growth of α-Alumina Nanocrystals on Mica. *Science* **1993**, *260*, 656–659.
19. Viswanathan, R.; Zasadzinski, J.; Schwartz, D. Strained-Layer van der Waals Epitaxy in a Langmuir–Blodgett Film. *Science* **1993**, *261*, 449–452.
20. Newton, M. C.; Warburton, P. A. ZnO Tetrapod Nanocrystals. *Mater. Today* **2007**, *10*, 50–54.
21. Fuller, M. L. Twinning in Zinc Oxide. *J. Appl. Phys.* **1944**, *15*, 164–170.
22. Zhu, Y. C.; Bando, Y.; Xue, D. F.; Golberg, D. Nanocable-Aligned ZnS Tetrapod Nanocrystals. *J. Am. Chem. Soc.* **2003**, *125*, 16196–16197.
23. Hu, J. Q.; Bando, Y.; Golberg, D. Sn-Catalyzed Thermal Evaporation Synthesis of Tetrapod-Branched ZnSe Nanorod Architectures. *Small* **2005**, *1*, 95–99.
24. Manna, L.; Scher, E. C.; Alivisatos, A. P. Synthesis of Soluble and Processable Rod-, Arrow-, Teardrop-, and Tetrapod-Shaped CdSe Nanocrystals. *J. Am. Chem. Soc.* **2000**, *122*, 12700–12706.
25. Kaito, C.; Fujita, K.; Shiojiri, M. Growth of CdTe Smoke Particles Preapred by Gas Evaporation Technique. *J. Cryst. Growth* **1983**, *62*, 375–383.
26. Manna, L.; Milliron, D. J.; Meisel, A.; Scher, E. C.; Alivisatos, A. P. Controlled Growth of Tetrapod-Branched Inorganic Nanocrystals. *Nat. Mater.* **2003**, *2*, 382–385.
27. Jun, Y. W.; Lee, S. M.; Kang, N. J.; Cheon, J. Controlled Synthesis of Multi-armed CdS Nanorod Architectures Using Monosurfactant System. *J. Am. Chem. Soc.* **2001**, *123*, 5150–5151.
28. Chen, M.; Xie, Y.; Lu, J.; Xiong, Y. J.; Zhang, S. Y.; Qian, Y. T.; Liu, X. M. Synthesis of Rod-, Twinrod-, and Tetrapod-Shaped CdS Nanocrystals Using a Highly Oriented Solvothermal Recrystallization Technique. *J. Mater. Chem.* **2002**, *12*, 748–753.
29. Yan, H. Q.; He, R. R.; Pham, J.; Yang, P. D. Morphogenesis of One-Dimensional ZnO Nano- and Microcrystals. *Adv. Mater.* **2003**, *15*, 402–405.
30. Grebinski, J. W.; Hull, K. L.; Zhang, J.; Kosel, T. H.; Kuno, M. Solution-Based Straight and Branched CdSe Nanowires. *Chem. Mater.* **2004**, *16*, 5260–5272.
31. Kuno, M.; Ahmad, O.; Protasenko, V.; Bacinello, D.; Kosel, T. H. Solution-Based Straight and Branched CdTe Nanowires. *Chem. Mater.* **2006**, *18*, 5722–5732.
32. Jun, Y. W.; Jung, Y. Y.; Cheon, J. Architectural Control of Magnetic Semiconductor Nanocrystals. *J. Am. Chem. Soc.* **2002**, *124*, 615–619.
33. Wu, X.; Zheng, Y.; Qu, F. ZnS Nanorods with Tripod-like and Tetrapod-like Legs. *Adv. Nat. Sci.* **2010**, *1*, 035005.
34. Huang, M. H.; Mao, S.; Feick, H.; Yan, H. Q.; Wu, Y. Y.; Kind, H.; Weber, E.; Russo, R.; Yang, P. D. Room-Temperature Ultraviolet Nanowire Nanolasers. *Science* **2001**, *292*, 1897–1899.
35. Ayers, J. E. *Heteroepitaxy of Semiconductors: Theory, Growth, and Characterization*; CRC Press: Boca Raton, FL, 2007.
36. Ertekin, E.; Greaney, P. A.; Chrzan, D. C.; Sands, T. D. Equilibrium Limits of Coherency in Strained Nanowire Heterostructures. *J. Appl. Phys.* **2005**, *97*, 114325.
37. Glas, F. Critical Dimensions for the Plastic Relaxation of Strained Axial Heterostructures in Free-Standing Nanowires. *Phys. Rev. B* **2006**, *74*, 121302.
38. Shi, J.; Wang, X. Strain *versus* Dislocation Model for Understanding the Heteroepitaxial Growth of Nanowires. *J. Phys. Chem. C* **2010**, *114*, 2082–2088.
39. Shiojiri, M.; Kaito, C. Structure and Growth of ZnO Smoke Particles Prepared by Gas Evaporation Technique. *J. Cryst. Growth* **1981**, *52*, 173–177.
40. Iwanaga, H.; Fujii, M.; Takeuchi, S. Growth Model of Tetrapod Zinc Oxide Particles. *J. Cryst. Growth* **1993**, *134*, 275–280.
41. Nishio, K.; Isshiki, T.; Kitano, M.; Shiojiri, M. Structure and Growth Mechanism of Tetrapod-like ZnO Particles. *Philos. Mag. A* **1997**, *76*, 889–904.
42. Dai, Y.; Zhang, Y.; Wang, Z. L. The Octa-twin Tetraleg ZnO Nanostructures. *Solid State Commun.* **2003**, *126*, 629–633.
43. Ding, Y.; Wang, Z. L.; Sun, T. J.; Qiu, J. S. Zinc-Blende ZnO and Its Role in Nucleating Wurtzite Tetrapods and Twinned Nanowires. *Appl. Phys. Lett.* **2007**, *90*, 153510–153513.
44. Yeh, C. Y.; Lu, Z. W.; Froyen, S.; Zunger, A. Zincblende-Wurtzite Polytypism in Semiconductors. *Phys. Rev. B* **1992**, *46*, 10086–10097.
45. Adu, K. W.; Xiong, Q.; Gutierrez, H. R.; Chen, G.; Eklund, P. C. Raman Scattering as a Probe of Phonon Confinement and

Surface Optical Modes in Semiconducting Nanowires. *Appl. Phys. A: Mater. Sci. Process* **2006**, *85*, 287–297.
46. Xiong, Q.; Wang, J.; Reese, O.; Lew Yan Voon, L. C.; Eklund, P. C. Raman Scattering from Surface Phonons in Rectangular Cross-Sectional w-ZnS Nanowires. *Nano Lett.* **2004**, *4*, 1991–1996.
47. Peng, Z.; Hu, H.; Utama, M. I. B.; Wong, L. M.; Ghosh, K.; Chen, R.; Wang, S.; Shen, Z.; Xiong, Q. Heteroepitaxial Decoration of Ag Nanoparticles on Si Nanowires: A Case Study on Raman Scattering and Mapping. *Nano Lett.* **2010**, *10*, 3940–3947.
48. Zhang, J.; Peng, Z.; Soni, A.; Zhao, Y.; Xiong, Y.; Peng, B.; Wang, J.; Dresselhaus, M. S.; Xiong, Q. Raman Spectroscopy of Few-Quintuple Layer Topological Insulator Bi_2Se_3 Nanoplatelets. *Nano Lett.* **2011**, *11*, 2407–2414.
49. Zelaya-Angel, O.; Castillo-Alvarado, F. D.; Avendano-Lopez, J.; Escamilla-Esquivel, A.; Contreras-Puente, G.; Lozada-Morales, R.; Torres-Delgado, G. Raman Studies in CdS Thin Films in the Evolution from Cubic to Hexagonal Phase. *Solid State Commun.* **1997**, *104*, 161–166.
50. Warekois, E. P.; Mariano, A. N.; Gatos, H. C.; Lavine, M. C. Crystallographic Polarity in II–VI Compounds. *J. Appl. Phys.* **1962**, *33*, 690–696.
51. Uccelli, E.; Arbiol, J.; Magen, C.; Krogstrup, P.; Russo-Averchi, E.; Heiss, M.; Mugny, G.; Morier-Genoud, F. O.; Nygård, J.; Morante, J. R.; *et al.* Three-Dimensional Multiple-Order Twinning of Self-Catalyzed GaAs Nanowires on Si Substrates. *Nano Lett.* **2011**, *11*, 3827–3832.
52. Mariano, A. N.; Hanneman, R. E. Crystallographic Polarity of ZnO Crystals. *J. Appl. Phys.* **1963**, *34*, 384–388.
53. Ma, C.; Moore, D.; Ding, Y.; Li, J.; Wang, Z. L. Nanobelt and Nanosaw Structures of II–VI Semiconductors. *Int. J. Nanotechnol.* **2004**, *1*, 431–451.
54. Müller, K.; Chang, C. C. Electric Dipoles on Clean Mica Surfaces. *Surf. Sci.* **1969**, *14*, 39–51.
55. Chikawa, J. I.; Nakayama, T. Dislocation Structure and Growth Mechanism of Cadmium Sulfide Crystals. *J. Appl. Phys.* **1964**, *35*, 2493–2501.
56. Gerlach, R.; Polanski, G.; Rubahn, H. G. Modification of Electric Dipole Domains on Mica by Excimer Laser Irradiation. *Surf. Sci.* **1996**, *352*, 485–489.
57. Shimaoka, G. Structure and Epitaxy of Evaporated Cadmium Sulfide Films. *Thin Solid Films* **1971**, *7*, 405–414.
58. Utama, M. I. B.; Zhang, J.; Chen, R.; Xu, X.; Li, D.; Sun, H.; Xiong, Q. Synthesis and Optical Properties of II–VI 1D Nanostructures. *Nanoscale* **2012**, *4*, 1422–1435.